Published Online on 29 June 2016

Proc Indian Natn Sci Acad **82** No. 2 June Spl Issue 2016 pp. 183-200

DOI: 10.16943/ptinsa/2016/48412

Research Paper

St Venant Torsion and Bending of Prismatic Composite Shafts

BHUSHAN LAL KARIHALOO[1,*] AND QI-ZHI XIAO[2]
[1]*School of Engineering, Cardiff University, Cardiff, CF24 3AA, UK*
[2]*LUSAS FEA Ltd, Forge House, 66 High Street, Kingston-upon-Thames, KT1 1HN, UK*

(Received on 20 April 2016; Accepted on 28 April 2016)

This paper discusses the use of high-performance incompatible, enhanced-strain and hybrid stress elements for the St Venant torsion and bending of composite prismatic shafts, formulated in terms of the warping function. The properties of the shaft are uniform along its length but piece-wise constant and orthotropic across its cross-section. In order to analyse composite shafts whose microstructural details are difficult to be modelled directly by finite element discretisation, the two-scale asymptotic (or mathematical) homogenisation approach is also discussed; the resulting equilibrium equations can be readily solved by the aforementioned high-performance elements.

Keywords: Composite Shaft; Enhanced-strain Element; Homogenisation; Hybrid Stress Element; Incompatible Element; Bending; Torsion

Introduction

St Venant torsion and bending of prismatic shafts are fundamental problems in the theory of elasticity and of wide interest in engineering design, see e.g. Pilkey (2002). It is also an essential ingredient in the development of advanced (Timoshenko) beam theory with shear correction (Gruttmann and Wagner, 2001) and/or torsional warping (Battini and Pacoste, 2002; Gruttmann *et al*, 2000; Simo and Vu-Quoc, 1991).

Many useful analytical solutions for torsion and bending of isotropic homogeneous shafts have been presented in books on theory of elasticity, e.g. Timoshenko and Goodier (1969). Karihaloo and Hemp (1987) and Pilkey (2002) have discussed optimization of cross-sectional shapes of shafts. Most recently, Romano *et al*. (2012) revisited the St Venant beam theory under shear and torsion with special attention to the notions of shear and twist centres; they used Matlab to solve the boundary value problems for simple regions.

Development of finite element approaches for the analysis of St Venant torsion began almost at the same time as the finite element method itself. A detailed discussion of the various approaches can be found in Desai (1979). Many early finite elements are based on stresses or stress functions and are limited to simply connected cross-sections. Xiao *et al*. (1999) have introduced an optimised hybrid stress element; Karihaloo *et al*. (2001) have developed displacement-incompatible and enhanced-strain elements. These high-performance elements are applicable for simply as well as multiply connected cross-sections.

Since the pioneering work of Mason and Herrmann (1968) on the development of a triangular displacement element from the principle of minimum potential energy, many studies have been carried out on the finite element analysis of St Venant bending. Gruttmann *et al*. (1999) and Gruttmann and Wagner (2001) formulated St Venant bending in terms of the bending warping function, which can be solved in a similar manner to the torsional warping function. They introduced a displacement compatible element to solve for bending warping, and a method for computing the shear correction factors for Timoshenko beams with arbitrary cross-sections assuming uncoupling of the strain energy for bending and torsion, and equivalence

*Author for Correspondence: E-mail: *karihaloob@cardiff.ac.uk*

of the strain energy from the average and equilibrium shear stresses. Jog and Mokashi (2014) studied bending of isotropic homogeneous bars with special attention to the torsion effect caused by the shearing forces that do not pass through the shear centre.

Lekhnitskii (1963) has explored torsion and bending of orthotropic homogeneous beams with simply connected cross-sections, making recourse to stress functions. Kosmatka and Dong (1991) studied prismatic anisotropic beams using the Ritz method based on the principle of minimum potential energy.

Kourtis *et al*. (2009) formulated compatible elements based on a combined warping function for torsion and transverse shearing of isotropic or transversely isotropic materials. They assumed that the elastic and shear moduli are spatial functions across the cross-section and considered the effects of their gradients; Poisson's ratio was assumed to be constant. With the use of Matlab to solve the boundary value problems for simple regions, Barretta (2013) studied orthotropic St Venant beams with a spatially constant Poisson tensor and fibre-wise homogeneous moduli of elasticity and shear with special attention on shear and twist centres. Jog and Mokashi (2014) studied torsion of prismatic compound anisotropic bars using 4- and 9-node compatible elements. Mokos and Sapountzakis (2005) also studied bending of composite beams with constant Poisson's ratio and piece-wise constant moduli of elasticity and shear by a boundary element method.

For composite shafts whose microstructural details are difficult to model directly using the finite element discretisation, Karihaloo *et al*. (2001) introduced the two-level asymptotic (or mathematical) homogenisation approach for periodic microstructures to the analysis of torsion. Yuan *et al*. (2003) used two-level homogenisation to the topology optimisation of cross-section for composite shafts under St Venant torsion.

This paper will discuss the solution of St Venant torsion and bending of prismatic composite shafts via high-performance finite elements or two-scale homogenisation. For St Venant bending, the violation of the assumption of zero in-plane shear strain γ_{xy} over the cross-section by Gruttmann *et al*. (1999) and Gruttmann and Wagner (2001) as well as Kourtis *et al*. (2009) will be resolved; for two-scale homogenisation, the first order formulation of Karihaloo *et al*. (2001) will be generalised to higher order following Xiao and Karihaloo (2009).

This paper is organised as follows: we will first discuss the formulation of St Venant torsion of prismatic composite shafts in terms of the warping function and high-performance incompatible, strain-enhanced and hybrid stress elements for solving the warping function. This will be followed by the formulation of St Venant bending in terms of the warping function, highlighting its similarity to torsion. We will next discuss the two-scale homogenisation and finite elements for solving the resulting equilibrium equations; followed by numerical examples and finally conclusions and discussion.

St Venant Torsion of Prismatic Composite Shaft

Take the origin at the centroid of one end section, *z*-axis along the axis of the shaft, *x* and *y* axes coincide with the principal axes of the section and form a right hand system with *z*. Orthotropic materials are considered. The principal directions of orthotropy coincide with the coordinate axes. The material properties are uniform along the length, but can be piece-wise constant across the cross-section. The initial stresses and strains will be ignored in the derivation of St Venant solutions, but added in the development of high-performance elements.

Under the assumption that $\sigma_x = \sigma_y = \sigma_z = \tau_{xy} = 0$, the displacements corresponding to unit angle of twist per unit length are

$$u = -yz \tag{1}$$

$$v = xz$$

$$w = \varphi(x, y)$$

where $\varphi(x, y)$ is the warping function. The non-vanishing strains are

$$\gamma_{xz} = \varphi_{,x} - y$$

$$\gamma_{yz} = \varphi_{,y} + x \tag{2}$$

where a comma denotes partial differentiation. The non-vanishing stresses are

$$\tau_{xz} = G_{xz}(\gamma_{xz} - \gamma_{xz}^0) + \tau_{xz}^0$$

$$\tau_{yz} = G_{yz}(\gamma_{yz} - \gamma_{yz}^0) + \tau_{yz}^0 \tag{3}$$

where G_{xz} and G_{yz} are shear moduli; γ_{xz}^0 and γ_{yz}^0 are initial strains including thermal strains; τ_{xz}^0 and τ_{yz}^0 are initial stresses.

The equilibrium equation is

$$\tau_{xz,x} + \tau_{yz,y} = 0 \text{, in A} \tag{4}$$

and boundary condition is

$$\tau_{xz} n_x + \tau_{yz} n_y = 0 \text{, on } \partial\text{A} \tag{5}$$

where (n_x, n_y) is the unit outward normal to ∂A, with A the cross-section domain.

Denote the shear stress vectors

$$\boldsymbol{\tau} = \begin{Bmatrix} \tau_{xz} \\ \tau_{yz} \end{Bmatrix}, \boldsymbol{\tau}^0 = \begin{Bmatrix} \tau_{xz}^0 \\ \tau_{yz}^0 \end{Bmatrix} \tag{6}$$

and shear strain vectors

$$\boldsymbol{\gamma} = \begin{Bmatrix} \gamma_{xz} \\ \gamma_{yz} \end{Bmatrix} = \begin{Bmatrix} \varphi_{,x} - f_1(x,y) \\ \varphi_{,y} - f_2(x,y) \end{Bmatrix}, \boldsymbol{\gamma}^0 = \begin{Bmatrix} \gamma_{xz}^0 \\ \gamma_{yz}^0 \end{Bmatrix} \tag{7}$$

where $f_1(x, y) = y$ and $f_2(x, y) = x$, and modulus and compliance matrices

$$\mathbf{D} = \begin{bmatrix} G_{xz} & 0 \\ 0 & G_{yz} \end{bmatrix}, \mathbf{C} = \begin{bmatrix} 1/G_{xz} & 0 \\ 0 & 1/G_{yz} \end{bmatrix} \tag{8}$$

the potential functional whose stationary condition gives (4) and (5) can be written as

$$\Pi_p(\varphi) = \int_A \left[\frac{1}{2} \boldsymbol{\gamma}^2 \mathbf{D} \boldsymbol{\gamma} + (-\mathbf{D}\boldsymbol{\gamma}^0 + \boldsymbol{\tau}^0)^T \boldsymbol{\gamma} \right] dA \tag{9}$$

The Hellinger-Reissner functional whose stationary condition gives (2)-(5) can be written as

$$\Pi_{HR}(\varphi, \boldsymbol{\tau}) = \int_A \left[-\frac{1}{2} \boldsymbol{\tau}^T \mathbf{C} \boldsymbol{\tau} + \boldsymbol{\tau}^T (\boldsymbol{\gamma} - \boldsymbol{\gamma}^0 + \mathbf{C}\boldsymbol{\tau}^0) \right] dA \tag{10}$$

By relaxing the compatibility condition (2) in the potential functional (9), or employing Legendre transformation on the Hellinger-Reissner functional (10), one arrives at the 3-field Hu-Washizu functional

$$\Pi_{HW}(\varphi, \boldsymbol{\gamma}, \boldsymbol{\tau}) = \int_A \left[\frac{1}{2} \boldsymbol{\gamma}^T \mathbf{D} \boldsymbol{\gamma} - \boldsymbol{\tau}^T \left(\boldsymbol{\gamma} - \begin{Bmatrix} \varphi_{,x} - f_1 \\ \varphi_{,y} - f_2 \end{Bmatrix} \right) + (-\mathbf{D}\boldsymbol{\gamma}^0 + \boldsymbol{\tau}^0)^T \boldsymbol{\gamma} \right] dA \tag{11}$$

4-node Incompatible/Strain-enhanced Element

For the 4-node element shown in Fig. 1, the warping function is divided into a compatible part φ_q and an incompatible part φ_λ:

$$\varphi = \varphi_q + \varphi_\lambda \tag{12}$$

φ_q is interpolated from nodal values $\boldsymbol{q} = [\varphi_1, \varphi_2, \varphi_3, \varphi_4]^T$ using the bilinear shape functions N_i as

$$\varphi_q = \boldsymbol{N}\boldsymbol{q} \tag{13}$$

where

$$N = [N_1 N_2 N_3 N_4] \tag{14}$$

and

$$N_i = \frac{1}{4}(1 + \xi_i \xi)(1 + \eta_i \eta) \tag{15}$$

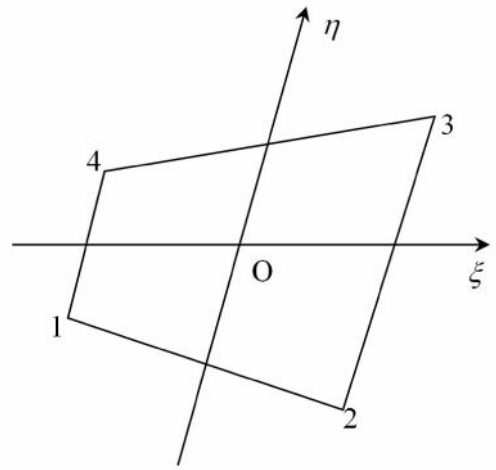

Fig. 1: A plane four-noded quadrilateral element

(ξ,η) represent the element isoparametric coordinates, (ξ_i,η_i) are the isoparametric coordinates of point i with the global coordinates $(x_i,y_i), i=1,2,3,4, \varphi_\lambda$ is related to the element inner parameters λ via the shape functions $\boldsymbol{N}_\lambda$

$$\varphi_\lambda = \boldsymbol{N}_\lambda \boldsymbol{\lambda} \tag{16}$$

Here, two incompatible terms are employed in each element as derived in Karihaloo *et al*. (2001) and Pian and Wu (2006)

$$\begin{aligned} &\boldsymbol{N}_\lambda = [N_{\lambda 1} N_{\lambda 2}] \\ &N_{\lambda 1} = \xi^2 - \Delta, N_{\lambda 2} = \eta^2 + \Delta \\ &\Delta = \frac{2}{3}\left(\frac{J_1}{J_0}\xi - \frac{J_2}{J_0}\eta\right) \end{aligned} \tag{17}$$

where J_0, J_1 and J_2 are related to the element Jacobian as follows

$$\begin{aligned} &|J| = J_0 + J_1\xi + J_2\eta = (a_1 b_2 - a_3 b_1) \\ &+(a_1 b_2 - a_2 b_1)\xi + (a_2 b_3 - a_3 b_2)\eta \end{aligned} \tag{18}$$

The coefficients and (i = 1, 2, 3) are dependent on the element nodal co-ordinates (x_i, y_i) (i = 1, 2, 3, 4) as follows:

$$\begin{vmatrix} a_1 & b_1 \\ a_2 & b_2 \\ a_3 & b_3 \end{vmatrix} = \frac{1}{4}\begin{vmatrix} -1 & 1 & 1 & -1 \\ 1 & -1 & 1 & -1 \\ -1 & -1 & 1 & 1 \end{vmatrix} \begin{vmatrix} x_1 & y_1 \\ x_2 & y_2 \\ x_3 & y_3 \\ x_4 & y_4 \end{vmatrix} \tag{19}$$

With the above assumed warping function (12) together with (13) and (16), we have the shear strains from (7)

$$\begin{aligned} \gamma = \begin{Bmatrix} \gamma_{xz} \\ \gamma_{yz} \end{Bmatrix} &= \begin{Bmatrix} \dfrac{\partial}{\partial x} \\ \dfrac{\partial}{\partial y} \end{Bmatrix} [\boldsymbol{N} \quad \boldsymbol{N}_\lambda] \begin{Bmatrix} \boldsymbol{q} \\ \boldsymbol{\lambda} \end{Bmatrix} + \begin{Bmatrix} -f_1 \\ f_2 \end{Bmatrix} \\ &= [\mathbf{B} \quad \mathbf{B}_\lambda] \begin{Bmatrix} \boldsymbol{q} \\ \boldsymbol{\lambda} \end{Bmatrix} + \begin{Bmatrix} -f_1 \\ f_2 \end{Bmatrix} \end{aligned} \tag{20}$$

Substituting (20) into (9) and making use of the stationary condition, yields

$$\tilde{\mathbf{K}}\boldsymbol{q} = \boldsymbol{f} \tag{21}$$

where the element stiffness matrix and nodal vector are

$$\tilde{\mathbf{K}} = \mathbf{K}_{qq} - \mathbf{K}_{q\lambda}\mathbf{K}_{\lambda\lambda}^{-1}\mathbf{K}_{q\lambda}^T, \quad \boldsymbol{f} = \mathbf{K}_{q\lambda}\mathbf{K}_{\lambda\lambda}^{-1}\boldsymbol{f}_\lambda - \boldsymbol{f}_q \tag{22}$$

in which

$$\begin{aligned} &\begin{bmatrix} \mathbf{K}_{qq} & \mathbf{K}_{q\lambda} \\ \mathbf{K}_{q\lambda}^T & \mathbf{K}_{\lambda\lambda} \end{bmatrix} = \int_A \begin{bmatrix} \mathbf{B}^T \\ \mathbf{B}_\lambda^T \end{bmatrix} \mathbf{D} [\mathbf{B} \quad \mathbf{B}_\lambda] dA \\ &\begin{Bmatrix} f_q \\ f_\lambda \end{Bmatrix} = \int_A \begin{bmatrix} \mathbf{B}^T \\ \mathbf{B}_\lambda^T \end{bmatrix} \left[\mathbf{D}\left(\begin{Bmatrix} -f_1 \\ f_2 \end{Bmatrix} - \gamma^0 \right) + \tau^0 \right] dA \end{aligned} \tag{23}$$

The element inner parameters λ are recovered as follows

$$\lambda = -\mathbf{K}_{\lambda\lambda}^{-1}\mathbf{K}_{q\lambda}^T\boldsymbol{q} - \mathbf{K}_{\lambda\lambda}^{-1}\boldsymbol{f}_\lambda \tag{24}$$

Alternatively, we can substitute the compatible bilinear interpolation of warping function in (13) and the shear strains (20) (the shear strains compatible with warping (13) are enhanced with $\mathbf{B}_\lambda\boldsymbol{\lambda}$) into the Hu-Washizu potential (11), an equivalent strain-enhanced element can be obtained.

4-node Hybrid Stress Element

In optimisation of the element trial stresses, the constant stresses are generally isolated to remain unperturbed to ensure the element is able to pass patch tests, see e.g., Pian and Wu (2005). Since St Venant torsion cannot have a constant shear stress field, in the development of the 4-node hybrid stress element, Xiao *et al*. (1999) did not isolate the constant shear stresses in optimisation of the element trial stresses and obtained the following optimised trial stresses

$$\begin{Bmatrix} \tau_{xz} \\ \tau_{yz} \end{Bmatrix} = \begin{bmatrix} a_1 b_3 - a_1 b_2 \xi & a_1 a_2 \xi & a_1\eta & a_3\xi \\ b_2 b_3 \eta & a_1 b_3 - a_2 b_3 \eta & b_1\eta & b_3\xi \end{bmatrix} \begin{Bmatrix} \beta_1 \\ \beta_2 \\ \beta_3 \\ \beta_4 \end{Bmatrix} \tag{25}$$

with 4 stress parameters β_1, β_2, β_3 and β_4. The trial stresses (25) satisfy the optimal parameter matching condition, and the resulting element performs as good

as the well-known Pian-Sumihara element for plane stress/strain problems (Pian and Sumihara, 1984).

However, the element with trial stresses (25) will fail for a square element with nodes numbered as in Fig. 2(a), which has nodal coordinates

$$x_1 = x_2 = -a,\ x_3 = x_4 = a,\ = y_1 = y_4 = a$$

$$\text{and } y_2 = y_3 = -a \tag{26}$$

giving

$$a_1 = a_2 = 0,\ a_3 = a \text{ and } b_1 = -a,\ b_2 = b_3 = 0 \tag{27}$$

with the use of (19). The trial stresses (25) become

$$\begin{Bmatrix}\tau_{xz}\\ \tau_{yz}\end{Bmatrix} = \begin{bmatrix}0 & 0 & 0 & a\xi\\ 0 & 0 & -a\eta & 0\end{bmatrix}\begin{Bmatrix}\beta_1\\ \beta_2\\ \beta_3\\ \beta_4\end{Bmatrix} \tag{28}$$

and the resulting **H** matrix (its definition is given in (37) below) will not be invertible. This problem can be resolved by renumbering the nodes into the pattern shown in Fig. 2(b), which gives

(A)

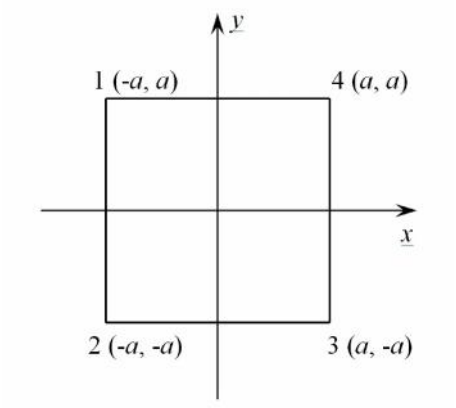

(B)

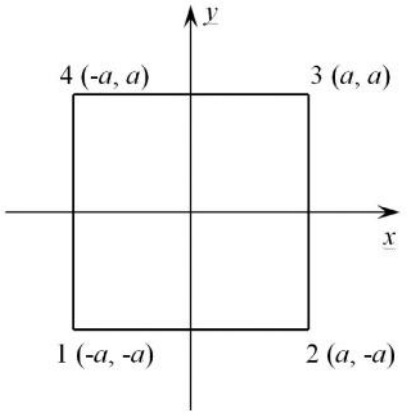

Fig. 2: Two typical node numbering patterns for a 4-node square element with side length 2*a*

$$x_1 = x_4 = -a,\ x_2 = x_3 = a,\ = y_2 = -a\ y_4 = a$$

$$\text{and } y_3 = y_4 = a \tag{29}$$

and

$$a_1 = a,\ a_2 = a_3 = 0,\ b_1 = b_2 = 0,\ b_3 = a \tag{30}$$

The trial stresses (25) become

$$\begin{Bmatrix}\tau_{xz}\\ \tau_{yz}\end{Bmatrix} = \begin{bmatrix}a^2 & 0 & a\eta & 0\\ 0 & a^2 & 0 & a\xi\end{bmatrix}\begin{Bmatrix}\beta_1\\ \beta_2\\ \beta_3\\ \beta_4\end{Bmatrix} \tag{31}$$

and the resulting **H** matrix will be invertible.

Alternatively, the constant shear stresses can be isolated from the stress optimisation procedure, and the initial assumed stresses of Xiao *et al*. (1999) can now be divided into constant and higher order parts as

$$\begin{Bmatrix}\tau_{xz}\\ \tau_{yz}\end{Bmatrix} = \begin{bmatrix}1 & 0 & \eta & 0 & \xi & 0\\ 0 & 1 & 0 & \xi & 0 & \eta\end{bmatrix}\begin{Bmatrix}\beta_1\\ \vdots\\ \beta_6\end{Bmatrix}$$

$$= \beta_c + [\varphi_I \,|\, \varphi_{II}]\begin{Bmatrix}\beta_I\\ \beta_{II}\end{Bmatrix}$$

$$\beta_c = \begin{Bmatrix}\beta_1\\ \beta_2\end{Bmatrix}, \beta_I = \begin{Bmatrix}\beta_3\\ \beta_4\end{Bmatrix}, \beta_{II} = \begin{Bmatrix}\beta_5\\ \beta_6\end{Bmatrix},$$

$$\varphi_I = \begin{bmatrix}\eta & 0\\ 0 & \xi\end{bmatrix}, \varphi_{II} = \begin{bmatrix}\xi & 0\\ 0 & \eta\end{bmatrix} \tag{32}$$

Enforcement of the stress optimisation condition on the higher order stresses $(\varphi_I \beta_I + \varphi_{II} \beta_{II})$ in (32) following Xiao *et al*. (1999) (or Pian and Wu (2005)) results in

$$\beta_{II} = \begin{bmatrix}0 & \dfrac{a_3}{b_3}\\ \dfrac{b_1}{a_1} & 0\end{bmatrix}\beta_I \tag{33}$$

Substitution of (33) into (32) gives the final optimised trial stresses

$$\begin{Bmatrix}\tau_{xz}\\ \tau_{yz}\end{Bmatrix} = \begin{bmatrix}1 & 0 & a_1\eta & a_3\xi\\ 0 & 1 & b_1\eta & b_3\xi\end{bmatrix}\begin{Bmatrix}\beta_1\\ \beta_2\\ \beta_3\\ \beta_4\end{Bmatrix}, \text{or } \tau = \phi\beta \tag{34}$$

Substitution of the warping function (13) into (7) gives the shear strain vector

$$\gamma = \mathbf{J}^{-1}\begin{bmatrix}\boldsymbol{N}_{,\xi}\\ \boldsymbol{N}_{,\eta}\end{bmatrix}\boldsymbol{q} + \begin{Bmatrix}-y\\ x\end{Bmatrix} = \mathbf{B}\boldsymbol{q} + \begin{Bmatrix}-y\\ x\end{Bmatrix} \tag{35}$$

Substitution of (34) and (35) into (10) gives

$$\Pi_{HP}(\boldsymbol{q},\beta) = -\frac{1}{2}\beta^T \boldsymbol{H}\beta + \beta^T(\mathbf{G}\boldsymbol{q} + \hat{\boldsymbol{f}}) \tag{36}$$

where

$$\begin{aligned}\mathbf{H} &= \int_A \phi^T \mathbf{C}\phi\, dA\\ \mathbf{G} &= \int_A \phi^T \boldsymbol{B} dA\\ \hat{\boldsymbol{f}} &= \int_A \phi^T \left(\begin{Bmatrix}-\boldsymbol{f}_1\\ f_2\end{Bmatrix} - \boldsymbol{\gamma}^0 + \mathbf{C}\boldsymbol{\tau}^0\right) dA\end{aligned} \tag{37}$$

Vanishing of the first order variation of Π_{HR} (36) gives

$$-\mathbf{H}\beta + \mathbf{G}\boldsymbol{q} + \hat{\boldsymbol{f}} = 0,\ \beta^T\mathbf{G} = 0 \tag{38}$$

The stress parameters can be computed from the first equation of (38)

$$\beta = \mathbf{H}^{-1}\mathbf{G}\boldsymbol{q} + \mathbf{H}^{-1}\hat{\boldsymbol{f}} \tag{39}$$

Substitution of (39) into the second equation of (38) gives

$$\mathbf{G}^T\mathbf{H}^{-1}\mathbf{G}\boldsymbol{q} = -\mathbf{G}^T\mathbf{H}^{-1}\hat{\boldsymbol{f}} \tag{40}$$

or the stiffness matrix

$$\mathbf{K} = \mathbf{G}^T\mathbf{H}^{-1}\mathbf{G} \tag{41}$$

and nodal load vector

$$\boldsymbol{f} = -\mathbf{G}^T\mathbf{H}^{-1}\hat{\boldsymbol{f}} \tag{42}$$

of the element.

Numerical tests confirm that the element resulting from (34) performs as good as the original element using trial stresses (25), but does not require renumbering the nodes for the special pattern shown in Fig. 2(a).

St Venant Torsionless Bending of Prismatic Composite Shaft

Under the assumption that the normal strain ε_z is linear with respect to *x*, *y* and *z*, according to the elementary beam theory, and stresses σ_x, σ_y and τ_{xy} are neglected

$$\begin{aligned}\varepsilon_z &= (\hat{a}_1 + \hat{a}_2 z)x + (\hat{b}_1 + \hat{b}_2 z)y\\ \sigma_x &= \sigma_y = \tau_{xy} = 0\end{aligned} \tag{43}$$

where $\hat{a}_1, \hat{a}_2, \hat{b}_1$ and $\hat{b}_2$ are constants, the non-vanishing strains are related to the stresses as

$$\begin{aligned}\varepsilon_x &= -\frac{\nu_{zx}}{E_z}\sigma_z\\ \varepsilon_y &= -\frac{\nu_{zy}}{E_z}\sigma_z\\ \varepsilon_x &= -\frac{\nu_{zx}}{E_z}\sigma_z\\ \varepsilon_z &= \frac{1}{E_z}\sigma_z\\ \gamma_{yz} &= \frac{1}{G_{yz}}\tau_{yz}\\ \gamma_{xz} &= \frac{1}{G_{xz}}\tau_{xz}\end{aligned} \tag{44}$$

The displacements

$$\begin{aligned}u &= -\nu_{zx}\left[\frac{1}{2}(a_1 + \hat{a}_2 z)x^2 + (\hat{b}_1 + \hat{b}_2 z)xy)\right]\\ &\quad + g_1(y,z)\\ v &= -\nu_{zy}\left[(\hat{a}_1 + \hat{a}_2 z)xy + \frac{1}{2}(\hat{b}_1 + \hat{b}_2 z)y^2)\right]\\ &\quad + g_2(x,z)\\ w &= \left(\hat{a}_1 + \hat{a}_2 z + \frac{1}{2}\hat{a}_2 z^2\right)x\\ &\quad + \left(\hat{b}_0 + \hat{b}_1 z + \frac{1}{2}\hat{b}_2 z^2\right)y + \varphi(x,y)\end{aligned} \tag{45}$$

where $\hat{a}_0$ and $\hat{b}_0$ are constants; $\varphi(x,y)$ is the warping function due to bending, and

$$g_1(y,z) = \frac{1}{2} v_{zy}(\hat{a}_1 + \hat{a}_2 z) y^2 - h_1(z)$$
$$g_2(x,z) = \frac{1}{2} v_{zx}(\hat{b}_1 + \hat{b}_2 z) x^2 - h_2(z) \quad (46)$$

and functions $h_1(z)$ and $h_1(z)$ satisfy

$$h_{1,z} = \hat{a}_0 + \hat{a}_1 z + \frac{1}{2}\hat{a}_2 z^2$$
$$h_{2,z} = \hat{b}_0 + \hat{b}_1 z + \frac{1}{2} b_2 z^2 \quad (47)$$

The non-vanishing shear strains are

$$\gamma_{xz} = \varphi_{,x} - f_1(x,y) \text{ 、}$$
$$\gamma_{yz} = \varphi_{,y} - f_2(x,y) \quad (48)$$

where

$$f_1(x,y) = v_{zx}\left(\frac{1}{2}\hat{a}_2 x^2 + \hat{b}_2 xy\right) - \frac{1}{2} v_{zy}\hat{a}_2 y^2$$
$$f_2(x,y) = -v_{zy}\left(\hat{a}_2 xy + \frac{1}{2}\hat{b}_2 y^2\right) + \frac{1}{2} v_{zx}\hat{b}_2 x^2 \quad (49)$$

The shear stresses are related to the shear strains (48) in the same manner as (3) after adding the initial stresses and strains into (44) and satisfying the equilibrium equation

$$\tau_{xz,x} + \tau_{yz,y} = -\sigma_{z,z} = -E_z(\hat{a}_2 x + \hat{b}_2 y) = f_0(x,y), \text{ in } A \quad (50)$$

and boundary condition for stress free cylindrical surface (5).

Constants $\hat{a}_2$ and $\hat{b}_2$ must be known before solving for the warping function due to bending; they can be computed from the shear forces Q_x and Q_y as follows.

$$\hat{a}_2 = \frac{EI_{xx}Q_x - EI_{xy}Q_y}{EI_{yy}.EI_{xx} - (EI_{xy})^2},$$
$$\hat{b}_2 = \frac{EI_{yy}Q_y - EI_{xy}Q_x}{EI_{yy}.EI_{xx} - (EI_{xy})^2} \quad (51)$$

where

$$EI_{xx} = \int_A E_z y^2 dA, EI_{yy} = \int_A E_z x^2 dA, EI_{xy} = \int_A E_z xy dA \quad (52)$$

A comparison with the formulation of St Venant torsion discussed above shows that the present formulation for St Venant bending appears identical to torsion except that a body force $f_0(x,y)$ now appears. The 4-node quadrilateral incompatible/strain-enhanced and hybrid stress elements for torsion can thus be readily used for the analysis of St Venant bending.

The potential functional whose stationary condition gives (50) and (5) now becomes

$$\Pi_p(\varphi) = \int_A \left[\frac{1}{2}\gamma^T \mathbf{D}\gamma + (-\mathbf{D}\gamma^0 + \tau^0)^T\gamma + f_0\varphi\right] dA \quad (53)$$

The Hellinger-Reissner functional whose stationary condition gives (48) together with (3), (50) and boundary condition (5) becomes

$$\Pi_{HR}(\varphi,\tau) = \int_A \left[-\frac{1}{2}\tau^T \mathbf{C}\tau + \tau^T(\gamma - \gamma^0 + \mathbf{C}\tau^0) + f_0\varphi\right] dA \quad (54)$$

By relaxing the compatibility condition (48) in the potential functional (53), or employing Lengendre transformation on the Hellinger-Reissner functional (54), one arrives at the Hu-Washizu functional

$$\Pi_{Hw}(\varphi,\gamma,\tau) = \int_A \left[\frac{1}{2}\boldsymbol{\tau}^T\mathbf{D}\gamma - \tau^T\left(\gamma - \begin{Bmatrix}\varphi_{,x} & -f_1(x,y)\\ \varphi_{,y} & +f_2(x,y)\end{Bmatrix}\right)\right.$$
$$\left. +(-D\gamma^0 + \tau^0)^T\gamma + f_0\varphi\right] dA \quad (55)$$

Incompatible/Strain-enhanced Element

Substitution of (12) together with (13) and (16) into (48) gives the shear strains (20). Substitution of (20) into (53) yields (21)-(24) with the only difference that

$$\begin{Bmatrix} f_q \\ f_\lambda \end{Bmatrix} = \int_A \begin{bmatrix} \mathbf{B}^T \\ \mathbf{B}_\lambda^T \end{bmatrix}$$

$$\left[\mathbf{D}\left(\begin{Bmatrix} -f_1 \\ f_2 \end{Bmatrix} - \gamma^0\right) + \tau^0\right] dA + \int_A \begin{Bmatrix} \boldsymbol{N}^T \\ \boldsymbol{N}_\lambda^T \end{Bmatrix} f_0 dA \quad (56)$$

in place of (23).

Hybrid Stress Element

Substitution of the warping and shear stress interpolations (13) and (34) into (54) yields

$$\begin{aligned} \Pi_{HR}(\boldsymbol{q}, \beta) &= -\frac{1}{2}\beta^T \mathbf{H}\beta \\ &+\beta^T(\mathbf{G}\boldsymbol{q} + \hat{\boldsymbol{f}}) + \hat{\boldsymbol{f}}^T\boldsymbol{q} \end{aligned} \quad (57)$$

where **H**, **G** and $\hat{\boldsymbol{f}}$ are the same as (37), but

$$\hat{\boldsymbol{f}} = \int_A \boldsymbol{N}^T f_0 dA \quad (58)$$

Vanishing of the first order variation of Π_{HR} (57) gives

$$\begin{aligned} -\mathbf{H}\beta + \mathbf{G}\boldsymbol{q} + \hat{\boldsymbol{f}} &= 0 \\ \beta^T\mathbf{G} + \hat{\boldsymbol{f}}^T &= 0 \end{aligned} \quad (59)$$

From the first equation of (59) we can obtain the stress parameters in the same manner as (39), substitution of them into the second equation of (59) gives

$$\mathbf{G}^T\mathbf{H}^{-1}\mathbf{G}\boldsymbol{q} = -\mathbf{G}^T\mathbf{H}^{-1}\hat{\boldsymbol{f}} - \hat{\boldsymbol{f}} \quad (60)$$

The stiffness matrix is the same as (41), but the nodal load vector now becomes

$$\boldsymbol{f} = -\mathbf{G}^T\mathbf{H}^{-1}\hat{\boldsymbol{f}} - \hat{\boldsymbol{f}} \quad (61)$$

Two-scale Asymptotic Homogenisation

Assume the microstructure of the cross-section A^ε occupied by the composite material to be locally periodic with a period defined by a statistically homogeneous volume element, denoted by the representative unit cell (RUC) or volume element (RVE) with size *Y*, as shown in Fig. 3. In other words, the composite material is formed by a spatial repetition

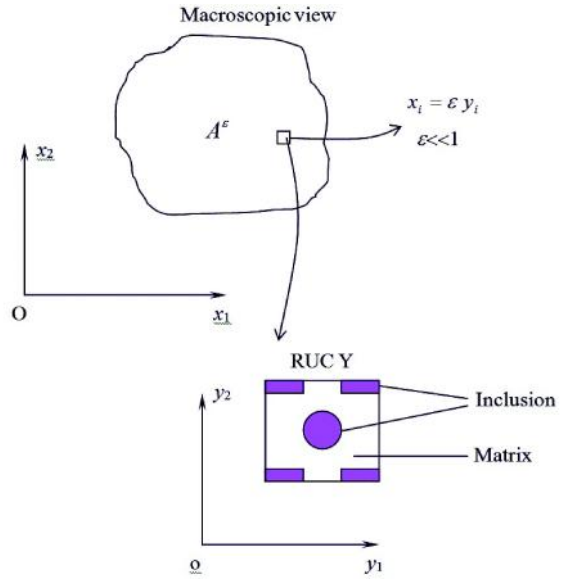

Fig. 3: Illustration of a problem with two length scales

of the RUC. The problem has two length scales; a global length scale *D* that is of the order of the size of section A^ε, and a local length scale *d* that is of the order of the RUC and proportional to the wavelength of the variation of the micro-structure. The size of the RUC is much larger than that of the constituents but much smaller than that of the section. The relation between the global coordinate system x_i for the section and the local system y_i for the minimum RUC can then be written as

$$y_i = \frac{x_i}{\varepsilon} i = 1,2 \quad (62)$$

where ε is a very small positive number representing the scaling factor between the two length scales. The local coordinate vector y_i is regarded as a stretched coordinate vector in the microscopic domain.

For an actual composite shaft subjected to external forces, field quantities such as warping function, shear strains and stresses are assumed to have slow variations from point to point with macroscopic (global) coordinate *x* as well as fast variations with local microscopic coordinate *y* within a small neighbourhood of size ε of a given point *x*

$$\begin{aligned} u_3^\varepsilon &= u_3^\varepsilon(x,y) = \varphi^\varepsilon(x,y) \\ \gamma_{3j}^\varepsilon &= \gamma_{3j}^\varepsilon(x,y) \\ \tau_{3j}^\varepsilon &= \tau_{3j}^\varepsilon(x,y) \end{aligned} \quad (63)$$

where $j = 1,2$. The superscript ε denotes Y-periodicity of the corresponding function.

The unknown displacement u_3^ε, the non-zero strain γ_{3j}^ε and stress τ_{3j}^ε can be solved from the following equations

Equilibrium:

$$\frac{\partial \tau_{3j}^\varepsilon}{\partial x_j} = f_0 \quad \text{in} \quad A^\varepsilon \tag{64}$$

where $f_0 = 0$ for torsion; it is defined as in (50) for bending.

Kinematical:

$$\begin{Bmatrix} \gamma_{31}^\varepsilon \\ \gamma_{32}^\varepsilon \end{Bmatrix} = \begin{Bmatrix} \dfrac{\partial u_3^\varepsilon}{\partial x_1} & f_1(x,y) \\ \dfrac{\partial u_3^\varepsilon}{\partial x_2} & f_2(x,y) \end{Bmatrix} \quad \text{in} \quad A^\varepsilon \tag{65}$$

Constitutive:

$$\tau_{3i}^\varepsilon = D_{ij}^\varepsilon \left(\gamma_{3j}^\varepsilon - \gamma_{3j}^0 \right) + \tau_{3j}^0 \quad \text{in} \quad A^\varepsilon \tag{66}$$

together with the traction free condition on the surface of the shaft, and the traction and displacement conditions at the interfaces between the micro-constituents. The material property tensor D_{ij}^ε is symmetric with respect to indices (i, j). The convention of summation over the repeated indices is used.

The displacement $u_3^\varepsilon(x,y)$ is expanded in powers of the small number e as

$$\begin{aligned} u_3^\varepsilon(x,y) &= u_3^{(0)}(x,y) + \varepsilon u_3^{(1)}(x,y) \\ &+ \varepsilon^2 u_3^{(2)}(x,y) + \varepsilon^3 u_3^{(3)}(x,y) .... \end{aligned} \tag{67}$$

where $u_3^{(0)}, u_3^{(1)}, u_3^{(2)}, ...,$ are Y-periodic functions with respect to y. Substituting (67) into (65) gives the expansion of the strain γ_{3j}^ε:

$$\gamma_{3j}^\varepsilon(x,y) = \varepsilon^{-1}\gamma_{3j}^{(-1)} + \gamma_{3j}^{(0)} + \varepsilon\gamma_{3j}^{(-1)} + ... \tag{68}$$

where

$$\begin{aligned} &\gamma_{3j}^{(-1)} = \frac{\partial u_3^{(0)}}{\partial y_j} \\ &\gamma_{3j}^{(0)} = \gamma_{x3j}^{(0)} + \gamma_{y3j}^{(0)}, \gamma_{x3j}^{(0)} = \frac{\partial u_3^{(0)}}{\partial x_1} - f_1. \\ &\gamma_{x32}^{(0)} = \frac{\partial u_3^{(0)}}{\partial x_1} + f_2, \gamma_{y3j}^{(0)} = \frac{\partial u_3^{(1)}}{\partial y_j} \\ &\gamma_{3j}^{(k)} = \frac{\partial u_3^{(k)}}{\partial x_j} + \frac{\partial u_3^{(k+1)}}{\partial y_j}, k \geq 1 \end{aligned} \tag{69}$$

Substituting (68) into the constitutive relation (66) gives the expansion of the stress τ_{3j}^ε

$$\tau_{3j}^\varepsilon(x,y) = \varepsilon^{-1}\tau_{3j}^{(-1)} + \tau_{3j}^{(0)} + \varepsilon\tau_{3j}^{(1)} + ... \tag{70}$$

where

$$\begin{aligned} &\tau_{3i}^{(-1)} = D_{ij}\gamma_{3j}^{(-1)} \\ &\tau_{3i}^{(0)} = D_{ij}\left(\gamma_{3j}^{(0)} - \gamma_{3j}^{(0)}\right) + \tau_{3j}^0 \\ &\tau_{3i}^{(k)} = D_{ij}\gamma_{3j}^{(k)}, k \geq 1 \end{aligned} \tag{71}$$

Inserting the asymptotic expansion for the stress field (70) into the equilibrium equation (64) and collecting the terms of like powers in ε gives the following sequence of equilibrium equations

$$O(\varepsilon^{-2}): \quad \frac{\partial \tau_{3j}^{(-1)}}{\partial y_j} = 0 \tag{72}$$

$$O(\varepsilon^{-1}): \quad \frac{\partial \tau_{3j}^{(-1)}}{\partial x_j} + \frac{\partial \tau_{3j}^{(0)}}{\partial y_j} = 0 \tag{73}$$

$$O(\varepsilon^{0}): \quad \frac{\partial \tau_{3j}^{(0)}}{\partial x_j} + \frac{\partial \tau_{3j}^{(1)}}{\partial y_j} = f_0 \tag{74}$$

$$O(\varepsilon^{k}): \quad \frac{\partial \tau_{3j}^{(k)}}{\partial x_j} + \frac{\partial \tau_{3j}^{(k+1)}}{\partial y_j} = 0, k \geq 1 \tag{75}$$

$O\left(\varepsilon^{-2}\right)$ *Equilibrium: Solution Structure of* $u_3^{(0)}$

We first consider the $O(\varepsilon^{-2})$ equilibrium equation (72) in Y. Pre-multiplying it by $u_3^{(0)}$, integrating over Y, followed by integration by parts, yields

$$\int_Y u_3^{(0)} \frac{\partial \tau_{3j}^{(-1)}}{\partial y_j} dY = \oint_{\partial Y} u_3^{(0)} \tau_{3j}^{(-1)} n_j d\Gamma -$$

$$\int_Y \frac{\partial u_3^{(0)}}{\partial y_j} D_{ji} \frac{\partial u_3^{(0)}}{\partial y_i} dY = 0 \tag{76}$$

where ∂Y denotes the boundary of Y. The boundary integral term in (76) vanishes due to the periodicity of the boundary conditions in Y, because $u_3^{(0)}$ and $\tau_{3j}^{(-1)}$ are identical on the opposite sides of the unit cell, while the corresponding normals d_j are in opposite directions. Taking into account the positive definiteness of the symmetric constitutive tensor D_{ij}, we have

$$\frac{\partial u_3^{(0)}}{\partial y_j} = 0 \Rightarrow u_3^{(0)} = u_3^{(0)}(x) \tag{77}$$

and

$$\gamma_{3j}^{(-1)}(x,y) = 0, \quad \tau_{3j}^{(-1)}(x,y) = 0 \tag{78}$$

$O\left(\varepsilon^{-1}\right)$ Equilibrium: First-Order Homogenisation and Solution Structure of $u_3^{(1)}$

Next, we proceed to the $O\left(\varepsilon^{01}\right)$ equilibrium equation (73). From (69) and (71) and taking into account (78), it follows that

$$\frac{\partial \tau_{3j}^{(0)}}{\partial y_j} = 0 \tag{79}$$

or

$$\frac{\partial}{\partial y_j}\left(D_{ji}\gamma_{y3i}^{(0)}(u_3^{(1)})\right) = -\frac{\partial D_{ji}}{\partial y_j}\left[\gamma_{x3i}^{(0)}(u_3^{(0)}) - \gamma_{3i}^0\right] \tag{80}$$

assuming that

$$\gamma_{3i}^0 = \gamma_{3i}^0(x), \tau_{3i}^0 = \tau_{3i}^0(x) \tag{81}$$

Based on the form of the right-hand side of (80) which permits a separation of variables, $u_3^{(1)}$ may be expressed as

$$u_3^{(1)}(x,y) = \chi_3^{3j}(v)\left[\gamma_{x3j}^{(0)}(u_3^{(0)}) - \gamma_{3j}^{(0)}\right] \tag{82}$$

where $\chi_3^{3j}(y)$ is a Y-periodic function defined in the unit cell Y. Substituting (82) into (80), and taking into account the arbitrariness of the macroscopic strain field, $\gamma_{x3j}\left(u_3^{(0)}\right) - \gamma_{3j}^0$ within a unit cell, we have

$$\frac{\partial}{\partial y_j}\left(D_{ji}\gamma_{y3i}^{(0)}(\chi_3^{3k}(y))\right) = -\frac{\partial D_{jk}}{\partial y_j} \tag{83}$$

We can also write

$$\tau_{3j}^{(0)} = D_{jl}\left(\delta_{\ln} + \frac{\partial \chi_3^{3n}}{\partial y_l}\right)\left(\gamma_{x3n}^{(0)} - \gamma_{3n}^0\right) + \tau_{3j}^0 \tag{84}$$

$O\left(\varepsilon^{0}\right)$ Equilibrium: Second-Order Homogenisation

We now consider the $O(\varepsilon^0)$ equilibrium equation (74).

Solution Structure of $u_3^{(2)}$

Without loss of generality, assume $\partial f_0 / \partial f_i = 0$. Differentiating equation (74) with respect to y_i gives

$$\frac{\partial^2 \tau_{3j}^{(0)}}{\partial y_i \partial x_j} + \frac{\partial^2 \tau_{3j}^{(1)}}{\partial y_i \partial y_j} = \frac{\partial f_0}{\partial y_i} = 0 \tag{85}$$

From (69) and (71), and making use of (82)

$$\tau_{3i}^{(i)} = D_{ij}\gamma_{3j}^{(1)} = D_{ij}\left(\frac{\partial u_3^{(1)}}{\partial x_j} + \frac{\partial u_3^{(2)}}{\partial y_j}\right)$$
$$= D_{ij}\left[\chi_3^{3n}(\mathbf{y})\frac{\partial}{\partial x_j}(\gamma_{x3n}^{(0)}(u_3^{(0)}) - \gamma_{3n}^0(\mathbf{x})) + \frac{\partial u_3^{(2)}}{\partial y_j}\right] \tag{86}$$

Making use of (84) and (86), we thus have

$$u_3^{(2)}(\mathbf{x},\mathbf{y}) = \psi_3^{3no}(\mathbf{y})\frac{\partial}{\partial x_o}(\gamma_{x3n}^{(0)}(u_3^{(0)}) - \gamma_{3n}^0(\mathbf{x}) \quad (87)$$

from (85).

Solution of u_3^0

Integrating (74) over the unit cell domain *Y* yields

$$\frac{\partial}{\partial x_j}\int_Y \tau_{3j}^{(0)} dY + \int_Y \frac{\partial \tau_{3j}^{(1)}}{\partial y_j} dY = \int_Y f_0 dY \quad (88)$$

Taking into account the periodicity of $\tau_{3j}^{(1)}$ on Y, the second term vanishes. Substituting (84) into (88) yields

$$\frac{\partial}{\partial x_j}\left\{\bar{D}_{jl}\left[\gamma_{x3l}^{(0)}\left(u_3^{(0)}\right) - \gamma_{3l}^0\right] + \tau_{3j}^0\right\} = f_0 \quad (89)$$

This is an equilibrium equation for a homogeneous medium (cf. (64)) with constant material properties $\bar{D}_{jl}$, which are usually termed as the homogenised or effective material properties and are given by

$$\bar{D}_{jn} = \frac{1}{Y}\int_Y \tilde{D}_{jn} dY, \tilde{D}_{jn} = \tilde{D}_{jl}\left(\delta_{ln} + \frac{\partial \chi_3^{3n}}{\partial y_l}\right) \quad (90)$$

where *Y* is the area of the unit cell.

In the widely used first-order homogenisation, displacements to order are solved; in a like manner the equations to order $O(\varepsilon^{-1})$ are considered. Equation (89) results from constraints from higher-order equilibrium and is used directly to solve for $u_3^{(0)}$. Hence no more constraints are required.

Solution of $\psi_3^{3no}(\mathbf{y})$

With the use of (84), (86), (87) and (90), (74) becomes

$$\frac{\partial}{\partial y_j}\left[D_{jl}\frac{\partial \Psi_3^{3no}(\mathbf{y})}{\partial y_1}\right]\frac{\partial}{\partial x_o}\left(\gamma_{x3n}^{(0)} - \gamma_{3n}^0\right) + \hat{f}_0 = 0 \quad (91)$$

where

$$f_0 = -f_0 + \frac{\partial}{\partial x_j}\left[D_{jl}\left(\gamma_{x3l}^{(0)} - \gamma_{3l}^0\right) + \tau_{3j}^0\right] +$$

$$+\frac{\partial}{\partial y_j}\left[D_{jl}\chi_3^{3n}(y)\right]\frac{\partial}{\partial x_i}\left(\gamma_{x3n}^{(0)} - \gamma_{3n}^0\right) \quad (92)$$

Constraints from Higher-Order Solutions

If the expansion is truncated to the second-order term $u_3^{(2)}$, its contribution to the $O(\varepsilon^1)$ order equilibrium equation needs also to be considered. The unwanted higher-order term $u_3^{(3)}$ in the equation can be eliminated by integrating the complete $O(\varepsilon^1)$ order equilibrium equation over Y. We thus have

$$\int_Y \left\{D_{jl}\left[\chi_3^{3n}(\mathbf{y})\delta_{lo} + \frac{\partial \psi_3^{3no}(y)}{\partial y_1}\right]\right\} dY.$$

$$\frac{\partial^2}{\partial x_j \partial x_o}\left(\gamma_{x3n}^{(0)}(u_3^{(0)}) - \gamma_{3n}^0\right) = 0 \quad (93)$$

or

$$\int_Y D_{jl}\frac{\partial \psi_3^{3no}(\mathbf{y})}{\partial y_1} dY = -\int_Y D_{jo}\chi_3^{3n}(\mathbf{y}) dY \quad (94)$$

$O(\varepsilon^1)$ Equilibrium: Third-Order Homogenisation

Solution of $u_3^{(3)}$

With the use of (69), (71) and (86), equation (75) becomes

$$\frac{\partial \tau_{3j}^{(1)}}{\partial x_j} + \frac{\partial \tau_{3j}^{(2)}}{\partial y_j} = \frac{\partial}{\partial x_j}$$

$$\left\{D_{jl}\left[\chi_3^{3n}(\mathbf{y})\frac{\partial}{\partial x_1}\left(\gamma_{x3n}^{(0)}(u_3^{(0)}) - \gamma_{3n}^0\right) + \frac{\partial u_3^{(2)}}{\partial y_1}\right]\right\}$$

$$+\frac{\partial}{\partial y_j}\left\{D_{jl}\left[\frac{\partial u_3^{(2)}}{\partial x_1} + \frac{\partial u_3^{(3)}}{\partial y_1}\right]\right\} = 0 \quad (95)$$

Assume D_{ij} is not explicitly dependent on **x**, $u_k^{(3)}$ can also be separated into **x**- and **y**-dependent terms

$$u_3^{(3)} = \phi_3^{3nop}(y)\frac{\partial^2}{\partial x_p \partial x_o}\left(\gamma_{x3n}^{(0)} - \gamma_{3n}^{0}\right) \tag{96}$$

(95) can be rewritten into the following equations

$$\frac{\partial}{\partial y_j}\left(D_{jl}\frac{\partial u_3^{(3)}}{\partial y_1}\right) - f_0^{(3)} = 0 \tag{97}$$

where

$$f_0^{(3)} = -\frac{\partial}{\partial x_j}$$
$$\left\{D_{jl}\left[\chi_3^{3n}(\mathbf{y})\frac{\partial}{\partial x_1}\left(\gamma_{x3n}^{(0)} - \gamma_{3n}^{0}\right) + \frac{\partial u_3^{(2)}}{\partial y_1}\right]\right\}$$
$$-\frac{\partial}{\partial y_j}\left\{D_{jl}\frac{\partial u_3^{(2)}}{\partial x_1}\right\} \tag{98}$$

Constraints from Higher-Order Terms

For the same reason as in solving for $u_3^{(2)}$, we need also to consider the $O(\varepsilon^2)$ order equilibrium equation. Again, integration of the complete $O(\varepsilon^2)$ order equilibrium equation over Y gives

$$\frac{\partial}{\partial x_j}\int_Y \left\{D\left[\psi_3^{3no}(\mathbf{y})\frac{\partial^2}{\partial x_1 \partial x_o}\left(\gamma_{x3n}^{(0)}(u_3^{(0)}) - \gamma_{3n}^{0}\right) + \frac{\partial u_3^{(3)}}{\partial y_1}\right]\right\} dY = 0 \tag{99}$$

or

$$\int_Y D_{jl}\frac{\partial \phi_3^{3nop}}{\partial y_1}dY = -\int_Y D_{jp}\psi_3^{3no}(\mathbf{y})dY \tag{100}$$

Obviously, terms higher than the third-order can be solved in a similar way. The controlling equations for the pth order ($p \geq 3$) displacements are

$$\frac{\partial}{\partial y_j}\left(D_{jl}\frac{\partial u_3^{(p)}}{\partial y_1}\right) - f_0^{(p)} = 0 \tag{101}$$

$$f_0^{(p)} = -\frac{\partial}{\partial x_j}\left\{D_{jl}\left[\frac{\partial u_3^{(p-2)}}{\partial x_1} + \frac{\partial u_3^{(p-1)}}{\partial y_1}\right]\right\}$$
$$-\frac{\partial}{\partial x_j}\left\{D_{jl}\frac{\partial u_3^{(p-1)}}{\partial x_1}\right\} \tag{102}$$

with constraints from higher order terms

$$\int_Y D_{jl}\left(\frac{\partial u_3^{(p-1)}}{\partial x_1} + \frac{\partial u_3^{(p)}}{\partial y_1}\right)dY = 0 \tag{103}$$

However, in the numerical implementation, although it is only required to solve a second-order equilibrium equation on the RUC (cf. (91) and (97)), it is actually limited by the requirement of the higher-order derivatives of the solution $u_3^{(0)}$ at the macro scale (cf. (92) and (98)).

Solution of Equilibrium Equations from Homogenisation

To solve the torsion or bending of composite shafts by the homogenisation method, we will first solve for $\chi_3^{3j}(y)$ from equation (83) assuming it to be a *Y*-periodic function defined in *Y*. The effective material properties $\bar{D}_{jk}$ are given by (90). We then solve the homogeneous St Venant torsion or bending problem (89) and obtain the macroscopic fields: warping displacement $u_3^{(0)}$, strains $\gamma_{x3j}^{(0)}$ and stresses (given by $\bar{D}_{jk}\,\gamma_{x3i}^{(0)}$). If the distribution of the microscopic fields in the neighborhood of point *x* is of interest, $u_3^{(1)}$ (82) can then be obtained from $\chi_l^{kl}(\mathbf{y})$ and $u_3^{(0)}$. $u_3^{(2)}$ can next be solved from (91) with constraints (93) or (94); $u_3^{(3)}$ can be solved from (97) with constraints (99) or (100). Higher-order displacement terms can be solved in a similar way. The strains γ_{3j} and stresses τ_{3j} can be calculated from (69) and (71), respectively. Equations (89), (91), (97) and (101) are standard second order partial differential equations in solid mechanics. They can be solved in a similar way. However, for a problem defined on the unit cell *Y* the periodic boundary conditions and constraints

from higher-order equilibrium should be enforced appropriately.

As all the equilibrium equations can be solved similarly, only equation (83) is discussed. Corresponding to (83), the virtual work principle states that

$$\int_Y \delta\chi_k^{3k} \frac{\partial}{\partial y_j}(D_{jl}\frac{\partial \chi_3^{3k}}{\partial y_1})dY + \int_Y \delta\chi_k^{3k}\frac{\partial D_{jk}}{\partial y_j}dY = 0 \tag{104}$$

or

$$\int_Y \frac{\partial \delta\chi_3^{3k}}{\partial y_j} D_{jl}\frac{\partial \chi_3^{3k}}{\partial y_1}dY + \int_Y \frac{\partial \delta\chi_3^{3k}}{\partial y_j} D_{jk}dY = 0$$

where $\delta\chi_3^{3k}$ are arbitrary *Y*-periodic functions defined in the unit cell *Y*.

It is easy to prove that (104) is the first order variation of the following potential functional

$$\Pi_p(\chi_3^{3k}) = \int_Y \frac{1}{2}\frac{\partial \chi_k^{3k}}{\partial y_j} D_{jl}\frac{\partial \chi_k^{3k}}{\partial y_i}dY + \int_Y \frac{\partial \chi_k^{3k}}{\partial y_j} D_{jk}dY \tag{105}$$

If we define the strain

$$\tilde{\gamma}_{3l}^k = \frac{\partial \chi_3^{3k}}{\partial y_i} \tag{106}$$

and the stress

$$\tilde{\tau}_{3j}^k = D_{jl}\tilde{\gamma}_{3l}^k \text{ so that } \tilde{\gamma}_{3l}^k = C_{ij}\tilde{\tau}_{3j}^k \tag{107}$$

which are Y-periodic functions in the unit cell, we have a 2-field Hellinger-Reissner functional

$$\Pi_{HR}(\chi_3^{3k}, \tilde{\tau}_{3j}^k) = \int_Y [-\frac{1}{2}\tilde{\tau}_{3j}^k C_{ij}\tilde{\tau}_{3j}^k + \tilde{\tau}_{3i}^k\frac{\partial \chi_3^{3k}}{\partial y_i} + D_{jk}\frac{\partial \chi_3^{3k}}{\partial y_j}]dY \tag{108}$$

By relaxing the compatibility condition in the potential (105) or by employing Legendre transformation on the Hellinger-Reissner (108) one arrives at the 3-field Hu-Washizu functional

$$\Pi_{HW}(\chi_3^{3k}, \tilde{\gamma}_{3j}^k, \tilde{\tau}_{3j}^k) = \int_Y [-\frac{1}{2}\tilde{\gamma}_{3i}^k D_{ij}\tilde{\gamma}_{3j}^k - \tilde{\tau}_{3i}^k(\tilde{\gamma}_{3j}^k - \frac{\partial \chi_3^{3k}}{\partial y_i}) + D_{jk}\frac{\partial \chi_3^{3k}}{\partial y_j}]dY \tag{109}$$

The general isoparametric compatible elements are not satisfactory because of the gradients of χ_3^{3k} that appear in (90) in the evaluation of the homogenised material properties. The shape functions in (12)-(17) can be adapted to interpolate χ_3^{3k} to formulate an equivalent displacement-incompatible element from the potential functional (105), or enhanced-strain element from the Hu-Washizu functional (109); adaption of the interpolation (13)-(15) for χ_3^{3k} and (34) for $\tilde{\tau}_{3i}^k$ can formulate an equivalent hybrid stress element from the Hellinger-Reissner functional (108).

Strictly speaking, solution of the Y-periodic functions on the RVE needs to satisfy the periodic conditions on the boundary, including the primary compatible displacement functions as well as the incompatible displacement/strain-enhanced terms for incompatible/strain-enhanced elements and assumed stresses for hybrid stress elements. The periodic constraints on compatible displacements can be imposed by a penalty function approach (Karihaloo *et al*. 2001; Xiao and Karihaloo, 2009), which can also be used to enforce the constraints from higher order terms; imposition of such constraints on incompatible displacements, enhanced-strains or stresses is difficult. However, numerical results (Feng and Wu, 2001; Karihaloo *et al*. 2001; Sun *et al*. 2001) show that neglecting the periodic constraints on these element internal fields does not deteriorate the solution.

Numerical Results

The performance of the incompatible/strain-enhanced element is almost identical to the hybrid stress element, we therefore only give the results from one of them in the following examples.

Torsion of Compound Square Shaft

Torsion of the compound square shaft of unit side

length composed of two equal in homogeneous regions shown in Fig. 4 with unit angle of twist per unit length is analysed. As in Ely and Zienkiewicz (1960) and Jog and Mokashi (2014), G_1 is fixed at 1 with E_1 = 2.5 and ν_1 = 0.25, three different values of G_2/G_1 = 1, 2 and 3 ($\nu_2 = \nu_1$) are considered. The cross-section is discretised into 88 four-node elements following Jog and Mokashi (2014); for the case G_2/G_1 = 3 a fine discretisation of 40×40 is also used. The torsional rigidities obtained by the hybrid stress element are compared against the analytical solution of Muskhelishvilli (1953), the relaxation finite difference method of Ely and Zienkiewicz (1960), and the 4-node element solution of Jog and Mokashi (2014) in Table 1. For a homogeneous shaft, the solution of Muskhelishvilli (1953) is identical to Timoshenko and Goodier (1969), as expected. The results from the hybrid stress element are the most accurate. The x-coordinate of the centroid and effective shear modulus are given in Table 2. The warping at A (–0.5, –0.25) and D (0.5, –0.25) relative to the centroid, and shear stresses at B (–0.5, 0) and C (0.5, 0) (Fig. 4) from the hybrid stress element are given in Table 3. For a homogeneous shaft, $G_2 = G_1$, the warping and shear stresses agree reasonably well with the analytical solutions $\varphi_A = -\varphi_D = 0.0347$, $\tau_{Cyz} = -\tau_{Byz} = 0.6753$ given by Timoshenko and Goodier (1969) despite the coarse mesh adopted. For the case G_2/G_1 = 3, the results from the coarse mesh agree well with those from the fine mesh.

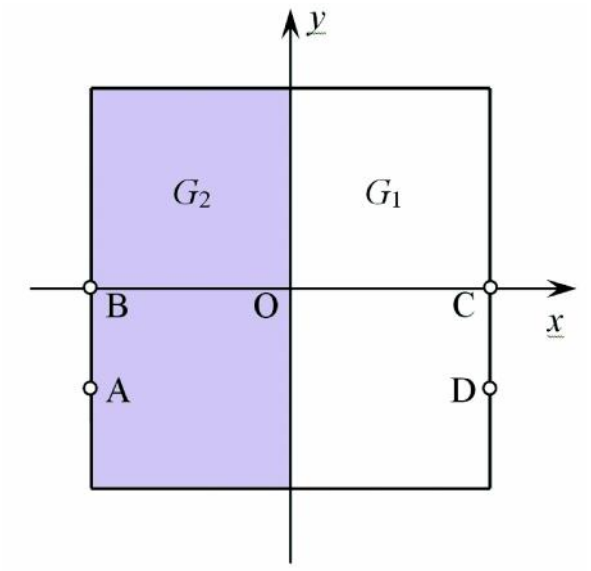

Fig. 4: Square cross-section of unit side length composed of two equal inhomogeneous regions

Table 1: Torsional rigidity for compound square shaft

G_2/G_1	Muskheli-shvilli (1953)	Ely and Zienkiewicz (1960)	Jog and Mokashi (2014)	Present hybrid element
1	0.1406	0.1388	0.1425	0.1398
2	0.1970	0.1941	0.1997	0.1957
3	0.2394	0.2358	0.2430	0.2377 (0.2396*)

*From refined discretisation 40x40

Table 2: x-coordinate of centroid and effective shear modulus

G_2/G_1	Discretisation	x_c	G_{eff}
1	8 x 8	0	1
2	8 x 8		1.3479
3	8 x 8	–0.125	1.5647
	40 x 40	–0.125	1.5628

Table 3: Warping and shear stresses for torsion of compound square shaft

G_2/G_1	Discretisation	φ at A	τ_{yz} at B	φ at D	τ_{yz} at C
1	8 x 8	0.03532	–0.6691	–0.03532	0.6691
2	8 x 8	0.04044	–1.2023	–0.03020	0.7370
3	8 x 8	0.04300	–1.7016	–0.02764	0.7709
	40 x 40	0.04224	–1.7102	–0.02728	0.7801

Bending of Compound Square Shaft

We now consider torsion-less bending of the above compound square shaft. The shear stresses given by the hybrid stress element at the centre are given in Table 4. Jump in the tangential stresses is noticed at the interface between different materials, and increases with the ratio G_2/G_1. For a homogeneous shaft, $G_2 = G_1$, the analytical solution is τ_{xz} = 1.4104 for Q_x = 1 and Q_y = 0, and = 1.4104 for Q_x = 0 and Q_y = 1 (Timoshenko and Goodier, 1969); the solution of the hybrid stress element agrees favourably with the analytical solution despite the coarse mesh adopted. In order to verify the accuracy of the hybrid stress element for inhomogeneous shafts, we analyse a cantilever of length 10 under transverse loading at the free end. The cantilever is divided into 16 x 16 (section) x 40 (length) 20-noded hexahedral elements. The results at the middle section are also included in

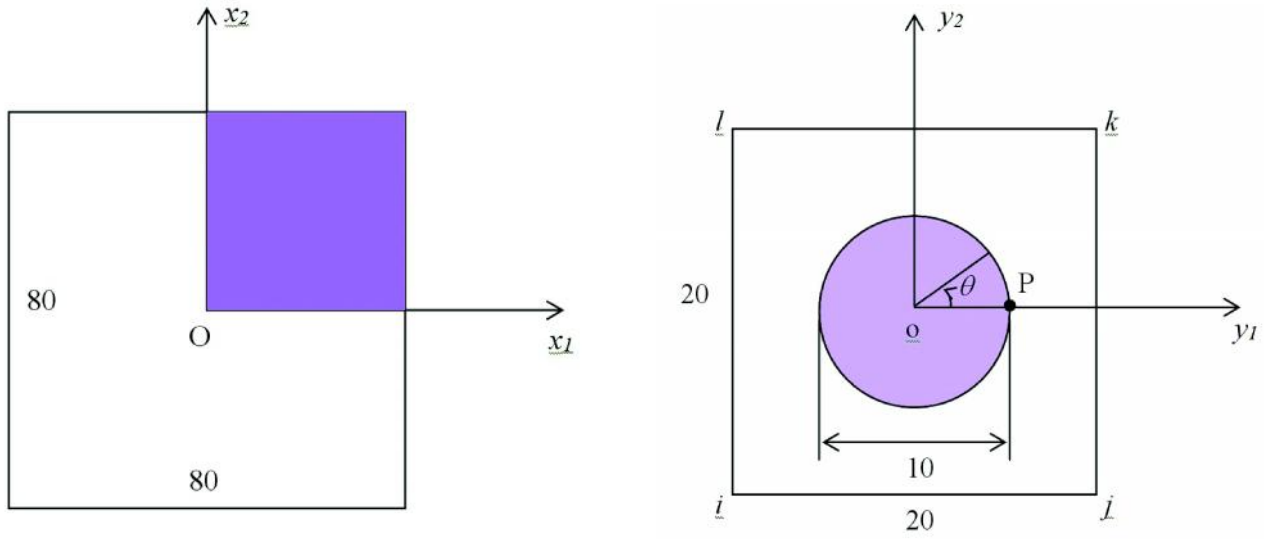

(A) (B)

Fig. 5: Geometry of a composite shaft of square profile (A) and RUC (B)

Table 4, agreeing reasonably with the hybrid stress element with the fine discretisation.

Torsion of a Square Composite Shaft

The example for the torsion of a composite shaft analysed by Karihaloo *et al*. (2001) is adopted to illustrate the first order homogenisation method. The composite shaft has a square cross-section (length of side = 80), as shown in Fig. 5(A); the microstructure of the cross-section is locally periodic with a period defined by a RUC shown in Fig. 5(B), i.e. it consists of an isotropic circular fibre of diameter 10 embedded in an isotropic square matrix with side 20. Assume that the scaling factor $\varepsilon = 0.25$. The problem is solved in two stages. First, we solve the RUC shown in Fig. 5(B) by using the incompatible/strain-enhanced element to obtain the field χ_3^{3k} and its derivatives $\frac{\partial}{\partial y_j}\chi_3^{3k}$ and calculate the homogenised moduli from (90). Second, we solve the torsion of the square shaft shown in Fig. 5(A) with the obtained homogenised moduli by using the hybrid stress element. Only a quarter of the cross-section, the shaded part shown in Fig. 5(A), is dicretised because of symmetry. The warping displacements are fixed on the axes of symmetry. In this way, we calculate the warping displacement, torsional rigidity and the angle of twist per unit length, as well as the shear stresses and strains. With the results so obtained, we can calculate the first order warping displacement from (82) and the local strain and stress fields from (69) and (71), respectively.

Table 4: Shear stresses at centre of compound square shaft under bending

G_2/G_1	Discretisation	$Q_x = 1$		$Q_y = 1$	
		left	right	left	right
1	8 x 8	1.3760	1.3760	1.3760	1.3760
2	8 x 8	1.3981	1.3024	1.8553	0.9277
3	8 x 8	1.3916	1.2297	2.1163	0.7054
	40 x 40	1.3289	1.2912	2.1658	0.7219
	1616 x 40†	1.3077	1.3038	2.3265	0.7755

† 20-noded hexahedral element

The shaded quarter in Fig. 5(A) is discretised into 400 quadrilateral elements and 441 nodes, as shown in Fig. 6(A). The RUC shown in Fig. 5(B) is discretised into 896 quadrilateral elements and 929 nodes, as shown in Fig. 6(B).

The fibre and the matrix are considered to be isotropic with the shear moduli, $G_f = 10$ and $G_m = 1$, respectively. The computed homogenised shear moduli are

$$\begin{bmatrix} C_{11} & C_{12} \\ Sym & C_{22} \end{bmatrix} = \begin{bmatrix} 1.38271 & -0.00138 \\ Sym & 1.38467 \end{bmatrix}$$

Thus the macroscopic behaviour of the composite shaft is also isotropic.

The isotropic shaft of square cross-section shown in Fig. 5(A) is now analysed with the obtained homogenised shear moduli. One unit of torque is applied on the quarter section with its units being consistent with those of the shear moduli. The computed result for the torsional rigidity 4 x 1.9927 x 10^6 is very close to the accurate value 7.9856 x 10^6 obtained from the formula $0.1406G(2b)^2$ where the shear modulus $G = 1.38271$, and the length of side of the square cross-section $2b = 80$ in the present example. The distribution of warping displacement, and of normal and tangential shear stresses, which are given by

$$\tau_n = \tau_{xz}\cos\theta + \tau_{yz}\sin\theta$$
$$\tau_t = -\tau_{xz}\sin\theta + \tau_{yz}\cos\theta$$

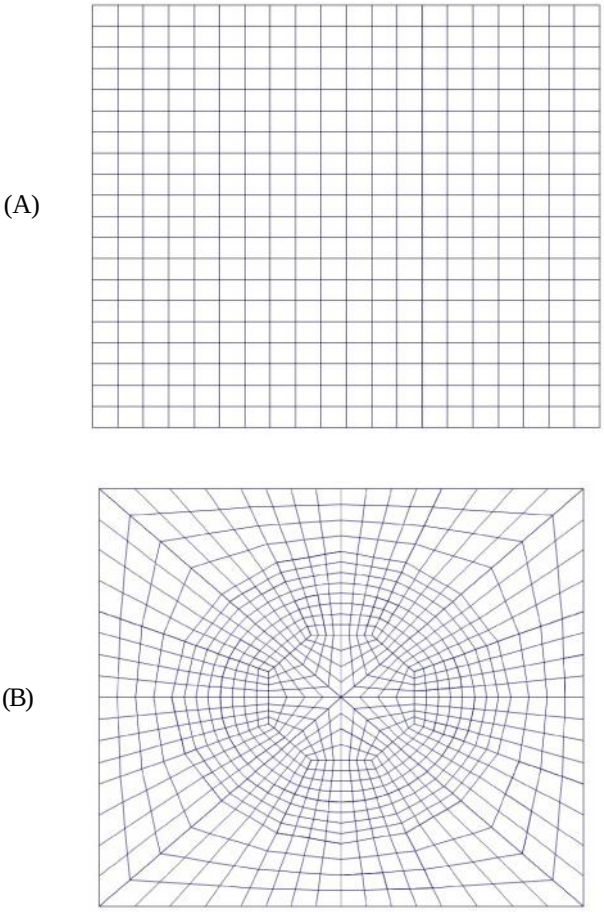

(A)

(B)

Fig. 6: Discretised meshes used in the computation: (A) Mesh of a quarter of the cross-section shown in Fig. 5(A); (B) Mesh of the RUC shown in Fig. 5(B)

where θ is the angle from the axis y_1 as shown in Fig. 5(B), along the interface between the fibre and the matrix adjacent to the point with global co-ordinates ($x_1 = 30, x_2 = 30$) are plotted in Fig. 7. Filled triangles represent computed data. In Fig. 7(B) and (C), data linked by broken lines represent the results obtained from the matrix side (a line segment represents the distribution of stress within an element), the continuous solid line represents the polynomial fit of the computed

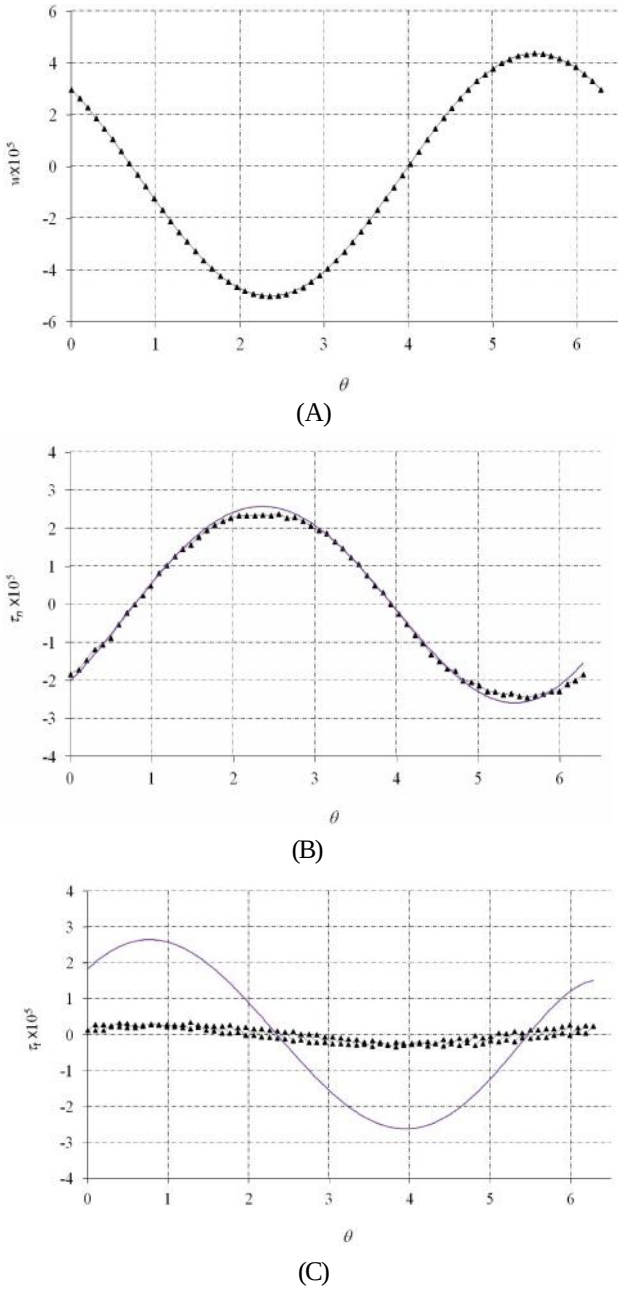

Fig. 7: Distribution of warping displacement (A), normal shear stress, (B) and tangential shear stress and (C) along the interface from the homogenisation method

results obtained from the fibre side of the interface since they are not satisfactorily smooth. From Fig. 7, the tangential shear stress τ_t has a significant discontinuity across the interface, while other fields are continuous adjacent to the interface.

Conclusions and Discussion

Formulation of the St Venant torsion of prismatic composite shafts with properties uniform along the length and piece-wise constant orthotropic across the cross-section is given in terms of the warping function. The principal axes of all constituents of the cross-section are assumed to be parallel. High-performance incompatible, strain-enhanced and hybrid stress elements for solving the warping function are discussed. In particular, a hybrid stress element developed earlier has been improved to avoid the need of a special node numbering pattern for square elements.

Formulation of the St venant bending (or shearing) of Gruttmann *et al*. (1999) and Gruttmann and Wagner (2001) for prismatic homogeneous isotropic shafts in terms of the warping function has been generalised to piece-wise constant orthotropic shafts; the requirement of zero in-plane shear strain over the cross-section, which is implicitly violated by the assumed strain field of Gruttmann *et al*. (1999) and Gruttmann and Wagner (2001), has been satisfied exactly in the present development. The warping function for bending can be solved by the same elements for the torsional warping function. Unlike Gruttmann *et al*. (1999) and Gruttmann and Wagner (2001), where the torsional warping function appears in the shear strains of bending and needs to be solved before the solution of bending, the formulation of bending in the present paper is purely in term of the warping function for bending.

In order to solve composite shafts for which the use of a finite element discretisation to represent all the microstructural details is too expensive or even impossible, the first order homogenisation for St Venant torsion (Karihaloo *et al*., 2001) has been generalised to higher order homogenisation following Xiao and Karihaloo (2009) for both St Venant torsion and bending; a more appropriate method is introduced to consider the constraints from higher order terms.

References

Barretta R (2013) On Cesàro-Volterra method in orthotropic Saint-Venant beam *J Elast* **112** 233-253

Battini J M and Pacoste C (2002) Co-rotational beam elements with warping effects in instability problems *Comput Methods Appl Mech Engrg* **191** 1755-1789

Bensoussan A, Lions J L and Papanicolaou G (2011) Asymptotic analysis for periodic structures *American Mathematical Soc*

Desai C S (1979) *Elementary finite element method* Englewood Cliffs: Prentice-Hall

Ely J F and Zienkiewicz O C (1960) Torsion of compound bars – a relaxation solution *Int J Mech Sci* **1** 356-365

Feng M L and Wu C C (2001) A study of three-dimensional four-step braided piezo-ceramic composites by the homogenization method *Compos Sci Tech* **61** 1889-1898

Gruttmann F, Sauer R and Wagner W (1999) Shear stresses in prismatic beams with arbitrary cross-sections *Int J Numer Meth Engng* **45** 865-889

Gruttmann, F, Sauer, R and Wagner, W (2000) Theory and numerics of three dimensional beams with elastoplastic material behaviour *Int J Numer Meth Engng* **48** 1675-1702

Gruttmann F and Wagner W (2001) Shear correction factors in Timoshenko's beam theory for arbitrary shaped cross-sections *Comput Mech* **27** 199-207

Jog C S and Mokashi I S (2014) A finite element method for the Saint-Venant torsion and bending problems for prismatic beams *Comput Struct* **135** 62-72

Karihaloo B L and Hemp W S (1987) Optimum shapes for given torsional and bending rigidities *Proc R Soc Lond* **A409** 67-77

Karihaloo, B L, Xiao Q Z and Wu C C (2001) Homogenization-based multivariable element method for pure torsion of composite shafts *Comput Struct* **79** 1645-1660

Kosmatka J B and Dong S B (1991) Saint-Venant solutions for prismatic anisotropic beams *Int J Solids Struct* **28** 917-938

Kourtis L C, Kesari H, Carter D R and Beaupré G S (2009) Transverse and torsional shear stresses in prismatic bodies having inhomogeneous material properties using a new 2D stress function *J Mech Mater Struct* **4** 659-674

Lekhnitskii S G (1963) Theory of Elasticity of an Anisotropic Elastic Body. Holden-Day

Mason W E and Herrmann L R (1968) Elastic shear analysis of general prismatic beams *J Eng Mech Div ASCE* **94** 965-986

Mokos V G and Sapountzakis E J (2005) A BEM solution to transverse shear loading of composite beams *Int J Solids Struct* **42** 3261-3287

Muskhelishvilli N I (1953) *Some basic problems of the mathematical theory of elasticity* Noordhoff, Groningen

Pian T H H and Sumihara K (1984) Rational approach for assumed stress finite elements *Int J Numer Meth Engng* **20** 1685-1695

Pian T H H and Wu C C (2006) *Hybrid and incompatible finite element methods* CRC Press

Pilkey W D **(**2002) *Analysis and design of elastic beams: Computational methods* John Wiley & Sons

Romano G, Barretta A and Barretta R (2012) On torsion and shear of Saint-Venant beams *Eur J Mech A/Solids* **35** 47-60

Simo J C and Rifai M S (1990) A class of mixed assumed strain methods and the method of incompatible modes *Int J Numer Meth Engng* **29** 1595-1638

Simo J C and Vu-Quoc L (1991) A geometrically-exact rod model incorporating shear and torsion-warping deformation *Int J Solids Struct* **27** 371-393

Sun H Y, Di S L, Zhang N and Wu C C (2001) Micromechanics of composite materials using multivariable finite element method and homogenization theory *Int J Solids Struct* **38** 3007-3020

Timoshenko S P and Goodier J N (1969) *Theory of elasticity* (3rd edition) McGraw-Hill

Wagner W and Gruttmann F (2001) Finite element analysis of Saint-Venant torsion problem with exact integration of the elastic-plastic constitutive equations *Comput Methods Appl Mech Engrg* **190** 3831–3848

Xiao Q Z and Karihaloo B L (2009) Two-scale asymptotic homogenisation-based finite element analysis of composite materials In: *Multiscale Modeling in Solid Mechanics: Computational Approaches* (Eds: Galvanetto U and Aliabadi M H F) pp 43-100, World Scientific

Xiao Q Z, Karihaloo B L, Li Z R and Williams F W (1999) An improved hybrid-stress element approach to torsion of shafts *Comput Struct* **71** 535-563

Yuan Z, Wu C C and Li H (2003) Homogenization-based topology design for pure torsion of composite shafts *Acta Mechanica Sinica* **19** 241-246.